

Sound-Pressure Level Calculations Using the RRA Algorithm for Depth-Dependent Speeds of Sound Valid at Turning Points and Focal Points

Lawrence J. Ziomek, *Senior Member, IEEE*

Abstract—Sound-pressure level (SPL) calculations are made along individual ray paths for arbitrary, one-dimensional, depth-dependent speeds of sound using an enhanced version of the RRA (recursive ray acoustics) algorithm. The SPL calculations are valid (i.e., finite) at turning points and focal points and do not require the use of Airy functions. The SPL calculations include the effects of frequency-dependent volume attenuation and frequency-dependent attenuation due to surface and bottom reflections. The ocean surface and bottom are treated as boundaries between viscous fluid media. Although the ocean surface is modeled as a planar boundary, the bathymetry is an arbitrary function of horizontal range. Sound speed versus depth and bathymetric data are represented by orthogonal function expansions. Computer simulation results from preliminary test cases are presented.

I. INTRODUCTION

IN a recent paper, Ziomek and Polnicky [1] introduced the RRA (recursive ray acoustics) algorithm. The RRA algorithm is simple, fast, and accurate (based on the preliminary test case results presented in [1]) and uses arc length as the independent variable. It can be used to compute the position, angles of propagation, travel time, and path length along a ray path for *three-dimensional* speeds of sound. Ziomek and Polnicky [1] did not discuss sound-pressure level (SPL) calculations.

The main purpose of this paper is to demonstrate how to use the output from the RRA algorithm to calculate the SPL along individual ray paths for arbitrary, one-dimensional, depth-dependent speeds of sound. Standard ray acoustics "correction formulas" for evaluating the acoustic field at a turning point or focal point for arbitrary, one-dimensional, depth-dependent speeds of sound require the use of Airy functions (e.g., see [2] and [3]). In contrast, the method used to perform SPL calculations in this paper is based on the approach presented by Krol [4]. Krol's method [4] does *not* require the use of Airy functions. Krol [4] demonstrated, via computer simulation results, intensity calculations along individual ray paths that were finite in value at both turning points and focal points. The computer simulation results reported by Krol [4] were for free-space propagation only, that is, the ray paths in his example encountered *no* surface and bottom reflections.

Although the RRA algorithm can handle three-dimensional speeds of sound, the method described by Krol [4] to calculate the intensity along a ray path is only applicable to one-dimensional, depth-dependent speeds of sound. However, the method of Gaussian beam tracing (e.g., see [5] and [6]) can be used to calculate the SPL not only for one-dimensional speeds of sound [5], but also for two- and three-dimensional speeds of sound [6]. The Gaussian beam method associates with each ray a beam with a Gaussian intensity profile normal to the ray. Auxiliary differential equations that govern the evolution of both the beam curvature and width are integrated along with the usual ray equations. In contrast, Krol's method [4] is based solely on one-dimensional ray acoustics—Gaussian intensity profiles are not artificially associated with individual ray paths.

The Gaussian beam method has the advantages of not requiring eigenray computations and not producing infinitely high intensity levels at caustics and zero intensity levels in shadow zones. However, the main disadvantage is that, at present, there is no agreed-upon method to compute the initial values for the beam width and curvature [5], [6]. Adjusting the initial conditions for the Gaussian beams can significantly alter the SPL at a receiver [5].

The SPL calculations discussed in this paper (see Section II) include the effects of frequency-dependent volume attenuation and frequency-dependent attenuation due to surface and bottom reflections. The ocean surface and bottom are treated as boundaries between viscous fluid media. Although the ocean surface is modeled as a planar boundary, the bathymetry is an arbitrary function of horizontal range. Sound speed versus depth and bathymetric data are represented by orthogonal function expansions (see Section III). Computer simulation results from preliminary test cases are presented in Section IV.

II. SPL CALCULATIONS

For an omnidirectional point source located at depth y_0 (see Fig. 10 in the Appendix), and for a speed of sound $c(y)$ an arbitrary function of depth y , the magnitude squared of the acoustic pressure along a ray path is given by (see Appendix)

$$|p(r, y)|^2 = |p(r_{01}, y_{01})|^2 \frac{\rho_0(y)c(y)}{\rho_0(y_{01})c(y_{01})} \frac{R_0^2 \sin \beta_0}{r |\cos \beta(y) dr/d\beta_0|} \quad (1)$$

Manuscript received April 2, 1993; revised September 20, 1993. This work was supported by NAVSEA.

The author is with the Department of Electrical and Computer Engineering, Naval Postgraduate School, Code EC/ZM, Monterey, CA 93943 USA.

IEEE Log Number 9216004.

U.S. Government Work Not Protected by U.S. Copyright

where

$$r = \sqrt{x^2 + z^2} \quad (2)$$

is the horizontal range, x and z are the cross-range and down-range coordinates, respectively,

$$r_{01} = R_0 \sin \beta_0, \quad (3)$$

$$y_{01} = y_0 + R_0 \cos \beta_0, \quad (4)$$

β_0 is the initial angle of propagation at the source, $\rho_0(y)$ is the depth-dependent ambient (equilibrium) density, and $\beta(y)$ is the angle of propagation (arrival) at depth y (see Fig. 10 in the Appendix). In order to evaluate (1), an equation for the denominator term $\cos \beta(y) dr/d\beta_0$ must be obtained.

Following the approach used by Krol [4], it can be shown that

$$D = \cos \beta(y) \frac{dr}{d\beta_0} = \cos \beta(y) \cot \beta_0 \int_{r_0}^r \frac{dr}{\cos^2 \beta(y)} \quad (5)$$

when

$$|\cos \beta(y)| > |c'(y)| \quad (6)$$

and

$$D = \cos \beta(y) \frac{dr}{d\beta_0} = \cot \beta_0 \sin \beta(y) \frac{c(y)}{c'(y)} + \cos \beta(y) \left[\cot \beta_0 \int_{r_0}^r \frac{\{c(y)c''(y) - [c'(y)]^2\}}{[c'(y)]^2} dr - \frac{c_0}{c'_0} \right] \quad (7)$$

when

$$|\cos \beta(y)| < |c'(y)| \quad (8)$$

where

$$c'(y) = \frac{d}{dy} c(y), \quad (9)$$

$$c''(y) = \frac{d^2}{dy^2} c(y), \quad (10)$$

$c_0 = c(y_0)$, $c'_0 = c'(y_0)$, and where it is understood that $y = y(r)$, that is, the horizontal range r along a ray path is the independent variable. The denominator term D given by (5) and (7) are *exact*—no additional simplifying assumptions or approximations were made. According to (8), (7) would be used, for example, whenever a ray path approached a turning point, that is, whenever $\beta(y) \rightarrow 90^\circ$, resulting in $\cos \beta(y) \rightarrow 0$. Note that if we let $R_0 = 1$ m, then $|p(r_{01}, y_{01})|^2$ appearing in (1) is related to the source level (SL) of the omnidirectional point source.

In order to make the calculation of $|p(r, y)|^2$ given by (1)–(10) compatible with the solution of the ray equations obtained from the RRA algorithm [1], the integrations over horizontal range r in (5) and (7) must first be transformed into

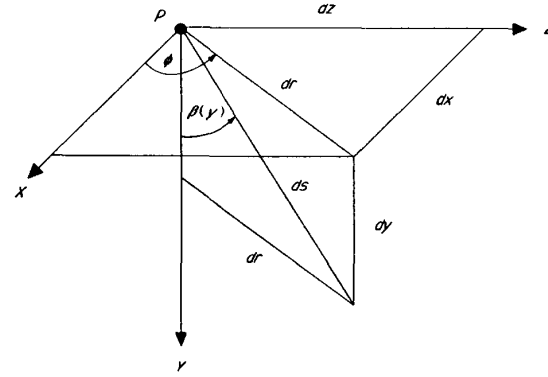


Fig. 1. An infinitesimal element of arc length ds at an arbitrary point P along a ray path.

integrations over the arc length s along a ray path (see Fig. 1). Recall that Snell's law is given by

$$\sin \beta(y) = bc(y) \quad (11)$$

where

$$b = \frac{\sin \beta_0}{c_0} \quad (12)$$

is the ray parameter. Therefore, by referring to Fig. 1 and using (11),

$$dr = \sin \beta(y) ds = bc(y) ds. \quad (13)$$

Also note that

$$v(y) = \cos \beta(y) \quad (14)$$

is the direction cosine with respect to the Y axis. With the use of (11)–(14), (5)–(8) can be rewritten as follows:

$$D = b \cot \beta_0 v(y) \int_0^s \frac{c(y)}{v^2(y)} ds \quad (15)$$

when

$$|v(y)| > |c'(y)| \quad (16)$$

and

$$D = b \cot \beta_0 \frac{c^2(y)}{c'(y)} + v(y) \left[b \cot \beta_0 \int_0^s \frac{c(y)\{c(y)c''(y) - [c'(y)]^2\}}{[c'(y)]^2} ds - \frac{c_0}{c'_0} \right] \quad (17)$$

when

$$|v(y)| < |c'(y)| \quad (18)$$

where it is understood that $y = y(s)$, that is, arc length s along a ray path is the independent variable.

Note that the RRA algorithm [1] already provides values for the cross-range x , depth y , down-range z , and the direction cosine v as functions of arc length s along a ray path, that is, $x = x(s)$, $y = y(s)$, $z = z(s)$, and $v(y) = v[y(s)]$. Therefore,

the horizontal range r along a ray path can also be expressed as a function of arc length, that is,

$$r = r(s) = \sqrt{x^2(s) + z^2(s)}. \quad (19)$$

However, to be more specific, the RRA algorithm [1] actually provides values for the aforementioned quantities as functions of step number i , that is, $x_i = x(s_i)$, $y_i = y(s_i)$, $z_i = z(s_i)$, and $v_i = v(y_i) = v[y(s_i)]$. Therefore, the magnitude squared of the acoustic pressure along a ray path can finally be expressed as follows:

$$|p(r_i, y_i)|^2 = |p(r_{01}, y_{01})|^2 \cdot \frac{\rho_0(y_i)c(y_i)}{\rho_0(y_{01})c(y_{01})} \frac{R_0^2 \sin \beta_0}{r_i |D_i|}, \quad i = 1, 2, 3, \dots \quad (20)$$

where

$$r_i = \sqrt{x_i^2 + z_i^2}. \quad (21)$$

Equation (15) is used when

$$|v_i| > |c'(y_i)| \quad (22)$$

and (17) is used when

$$|v_i| < |c'(y_i)|. \quad (23)$$

It is often convenient to express the values of acoustic pressure in terms of sound-pressure levels. The sound-pressure level (SPL) is defined as follows:

$$\text{SPL} \triangleq 20 \log_{10} \left(\frac{\sqrt{2}|p|/2}{P_{\text{ref}}} \right) \text{ dB re } P_{\text{ref}} \quad (24)$$

where $|p|$ is the magnitude of the acoustic pressure, P_{ref} is the root-mean-square (rms) reference pressure, and "re" means "relative to." For problems in underwater acoustics, $P_{\text{ref}} = 1 \mu\text{Pa}$ (rms) is common. Therefore, the SPL along a ray path as a function of step number i can be expressed as

$$\text{SPL}_i = 10 \log_{10} |p_i|^2 - \text{REFSPL dB re } P_{\text{ref}}, \quad i = 1, 2, 3, \dots \quad (25)$$

where $|p_i|^2 = |p(r_i, y_i)|^2$ is given by (20) and

$$\text{REFSPL} = 10 \log_{10} 2 + 20 \log_{10} P_{\text{ref}}. \quad (26)$$

The effects of frequency-dependent attenuation due to surface and bottom reflections can be modeled by using appropriate equations for the reflection coefficients at the ocean surface and bottom. If we designate the air as medium I, the ocean medium as medium II, and the ocean bottom as medium III, and since the sound source is in medium II, then the reflection coefficient at the ocean surface R_{21} and the reflection coefficient at the ocean bottom R_{23} are given by

$$R_{2m} = \frac{\rho_m \cos \zeta_{\text{inc}} - \rho_2 B_{2m}}{\rho_m \cos \zeta_{\text{inc}} + \rho_2 B_{2m}}, \quad m = 1, 3 \quad (27)$$

where ρ_m , $m = 1, 2, 3$ is the ambient (equilibrium) density in kilograms per cubic meter of media I, II, and III, respectively,

ζ_{inc} is the angle of incidence measured with respect to the local normal to the boundary at the point of incidence,

$$B_{2m} = \begin{cases} \sqrt{N_{2m}^2 - \sin^2 \zeta_{\text{inc}}}, & \text{Re}\{N_{2m}^2\} \geq \sin^2 \zeta_{\text{inc}}, \\ -j\sqrt{\sin^2 \zeta_{\text{inc}} - N_{2m}^2}, & \text{Re}\{N_{2m}^2\} < \sin^2 \zeta_{\text{inc}}, \end{cases} \quad m = 1, 3 \quad (28)$$

$$N_{2m} \triangleq \frac{K_m}{K_2}, \quad m = 1, 3 \quad (29)$$

is the complex index of refraction between media II and I, and II and III, respectively,

$$K_m = k_m - j\alpha_m(f), \quad m = 1, 2, 3 \quad (30)$$

is the complex wavenumber,

$$k_m = 2\pi f/c_m, \quad m = 1, 2, 3 \quad (31)$$

is the real wavenumber in radians per meter, c_m is the speed of sound in meters per second, and $\alpha_m(f)$ is the real, frequency-dependent attenuation coefficient in nepers per meter in media I, II, and III, respectively. Note that for ideal, nonviscous fluids, $\alpha_m(f) = 0$, $m = 1, 2, 3$. The right-hand side of (20) is multiplied by the magnitude squared of either R_{21} or R_{23} in order to take into account the effects of a surface or bottom reflection, respectively.

In addition, the effect of frequency-dependent volume attenuation can be modeled by multiplying the right-hand side of (20) by $\exp[-2\alpha_2(f)s_i]$, where $\alpha_2(f)$ is the frequency-dependent attenuation coefficient of the ocean medium in Np/m and s_i is the value of the arc length along a ray path at step number i (an output of the RRA algorithm). The factor of 2 is present in the exponent because (20) is an expression for the magnitude squared of the acoustic pressure.

III. ORTHOGONAL FUNCTION EXPANSIONS OF SOUND SPEED AND BATHYMETRIC DATA

In this section, we shall discuss why and how sound speed versus depth data and bathymetry versus horizontal range data are represented by orthogonal function expansions. Measured data are usually noise corrupted. Even in the absence of noise, data are uncertain due to the lack of precision in the measurement equipment. As a result, if an interpolation scheme such as cubic splines is used to fit noise corrupted and/or uncertain measured data, then the noise and/or the uncertainty in the data are being fit rather than the trend in the data since an interpolation scheme will pass a curve through each data point.

When dealing with noise-corrupted and/or uncertain data, it is better to fit the data using an orthogonal function expansion. An orthogonal function expansion will fit the data in a minimum mean-squared error (MMSE) sense using orthogonal polynomials. It is analogous to, but *not* the same as, the method of nonlinear least squares estimation. The order of the orthogonal function expansion of the data can be increased by simply computing the next higher order coefficient—all previous coefficients do *not* have to be recomputed. In addition, the data do *not* have to be evenly spaced.

Let $c_m(y_i)$, $i = 1, 2, \dots, M_c$ represent the measured sound speed versus depth data, where M_c is the total number of measured sound-speed data points. Using the measured data, an estimate $\hat{c}(y)$ of the speed of sound $c(y)$ can be obtained from the following N_c th-order orthogonal function expansion:

$$\hat{c}(y) = \sum_{n=0}^{N_c} c_n \varphi_{cn}(y), \quad 0 \leq y \leq D \quad (32)$$

where the coefficient

$$\begin{aligned} c_n &= \langle c_m(y_i), \varphi_{cn}(y_i) \rangle \\ &= \sum_{i=1}^{M_c} c_m(y_i) \varphi_{cn}^*(y_i), \quad n = 0, 1, \dots, N_c. \end{aligned} \quad (33)$$

The angular brackets denote inner product and the asterisk "*" denotes complex conjugate. The set of basis functions $\varphi_{cn}(y)$, $n = 0, 1, \dots, N_c$ are *orthonormal* in the interval $0 \leq y \leq D$ and were determined by using the Gram-Schmidt procedure [7] on the set of real functions $f_n(y) = y^n$, $n = 0, 1, 2, \dots$.

Similarly, let $y_{bm}(r_i)$, $i = 1, 2, \dots, M_b$ represent the measured ocean bottom depth versus horizontal range data, where M_b is the total number of measured bathymetric data points. Using the measured data, an estimate $\hat{y}_b(r)$ of the bathymetry $y_b(r)$ can be obtained from the following N_b th-order orthogonal function expansion:

$$\hat{y}_b(r) = \sum_{n=0}^{N_b} b_n \varphi_{bn}(r), \quad 0 \leq r \leq R \quad (34)$$

where the coefficient

$$\begin{aligned} b_n &= \langle y_{bm}(r_i), \varphi_{bn}(r_i) \rangle \\ &= \sum_{i=1}^{M_b} y_{bm}(r_i) \varphi_{bn}^*(r_i), \quad n = 0, 1, \dots, N_b. \end{aligned} \quad (35)$$

The set of basis functions $\varphi_{bn}(r)$, $n = 0, 1, \dots, N_b$ are *orthonormal* in the interval $0 \leq r \leq R$ and were determined by using the Gram-Schmidt procedure [7] on the set of real functions $f_n(r) = r^n$, $n = 0, 1, 2, \dots$.

In order to determine the order N_c and N_b to be used for the orthogonal function expansion of both the sound speed and bathymetric data, respectively, the following procedure is used. Since the procedure is the same for both the sound speed and bathymetric data, we shall explain it for the sound-speed data only. Using the measured sound speed versus depth data, an estimate of the speed of sound $\hat{c}(y)$ given by (32) is obtained for *all* allowed values of N_c where, in this paper, $N_c = 0, 1, \dots, 5$. For each value of N_c , the mean-squared error MSE_c is computed as follows:

$$MSE_c = E_{c_m} - E_{\hat{c}} \quad (36)$$

where

$$E_{c_m} = \langle c_m(y_i), c_m(y_i) \rangle = \sum_{i=1}^{M_c} |c_m(y_i)|^2 \quad (37)$$

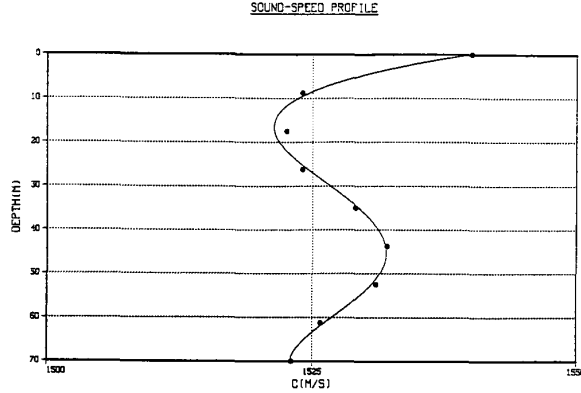


Fig. 2. Curve fit of sound-speed data using the orthogonal function expansion given by (32).

is the energy contained in the measured sound-speed data, and

$$E_{\hat{c}} = \langle \hat{c}(y_i), \hat{c}(y_i) \rangle = \sum_{i=1}^{M_c} |\hat{c}(y_i)|^2 \quad (38)$$

is the energy contained in the sound-speed estimate. The value of N_c that produces the *minimum* value of MSE_c becomes the order of the expansion used in (32).

Similarly,

$$MSE_{y_b} = E_{y_{bm}} - E_{\hat{y}_b} \quad (39)$$

where

$$E_{y_{bm}} = \langle y_{bm}(r_i), y_{bm}(r_i) \rangle = \sum_{i=1}^{M_b} |y_{bm}(r_i)|^2 \quad (40)$$

is the energy contained in the measured bathymetric data, and

$$E_{\hat{y}_b} = \langle \hat{y}_b(r_i), \hat{y}_b(r_i) \rangle = \sum_{i=1}^{M_b} |\hat{y}_b(r_i)|^2 \quad (41)$$

is the energy contained in the bathymetric estimate given by (34) where $N_b = 0, 1, \dots, 5$.

Figs. 2 and 3 are examples of curve fits to sound speed and bathymetric data obtained by using the orthogonal function expansions given by (32) and (34), respectively. In both Figs. 2 and 3, the black dots represent the original, unevenly spaced data points. As can be seen from both of these figures, the curves do not pass through all of the data points. Instead, the curves fit the trend of the data in a MMSE sense.

IV. COMPUTER SIMULATION RESULTS

Computer simulation results for three test cases are reported in this paper. *Test case 1* simulated ray propagation in an ocean waveguide with a 3° up-slope bottom. The ocean surface and bottom were modeled as ideal pressure-release and rigid boundaries, with reflection coefficients $R_{21} = -1$ and $R_{23} = 1$, respectively. The ocean medium was modeled as being nonviscous with constant speed of sound $c_2 = 1500$ m/s. The sound source was placed at a depth of $y_0 = 150$ m with a $SL = 180$ dB re $1 \mu\text{Pa}$ (rms). Two rays were transmitted

OCEAN BOTTOM BATHYMETRY

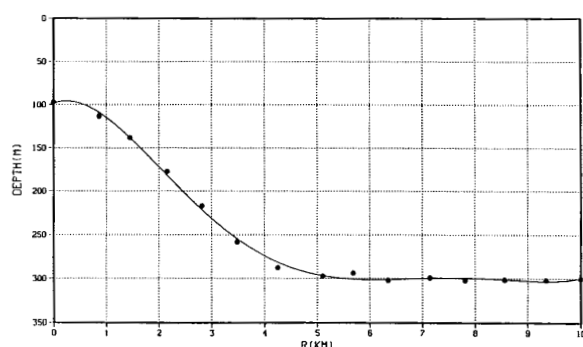


Fig. 3. Curve fit of bathymetric data using the orthogonal function expansion given by (34).

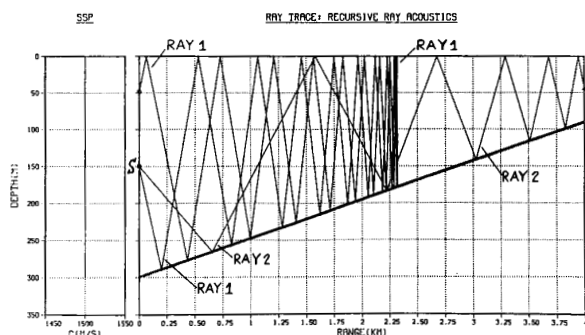


Fig. 4. Ray trace for test cases 1 and 2. 3° up-slope bottom with sound source (S) at a depth of $y_0 = 150$ m. Two rays are transmitted with initial angles of propagation $\beta_0 = 55^\circ$ (ray 1) and 80° (ray 2).

from the source with initial angles of propagation $\beta_0 = 55^\circ$ and 80° . An arc length step size of 2 m was used. Figs. 4 and 5 illustrate the corresponding ray trace and SPL plots for test case 1. From Fig. 4, it can be seen that both rays "compress" as they propagate up-slope, as predicted by theory. However, the first ray ($\beta_0 = 55^\circ$) turns back on itself at $r \approx 2.3$ km and propagates back toward the source, arriving at $r = 0$ km with a depth of $y \approx 50$ m. This phenomenon of rays turning back on themselves and propagating back toward the sound source is also predicted by theory for up-slope propagation. Although both rays shown in Fig. 4 underwent many surface and bottom reflections, since the ocean surface and bottom were modeled as ideal pressure-release and rigid boundaries, the corresponding SPL plots shown in Fig. 5 are smooth with no discontinuities. In addition, since the ocean medium was modeled as being nonviscous with a constant speed of sound, the SPL decreased at the expected rate of 6 dB for each doubling of the range.

Test case 2 is identical to test case 1, with the exception that medium II (ocean water) and medium III (ocean bottom) were modeled as viscous fluid media using the following parameter values: $\rho_1 = 1.21 \text{ kg/m}^3$, $c_1 = 343 \text{ m/s}$, and $\alpha_1(f) = 0 \text{ dB/m}$ (0 Np/m); $\rho_2 = 1026 \text{ kg/m}^3$, $c_2 = 1500 \text{ m/s}$, and $\alpha_2(f) = 0.625 \times 10^{-5} \text{ dB/m}$ ($0.7195 \times 10^{-6} \text{ Np/m}$)

SPL: RECURSIVE RAY ACOUSTICS

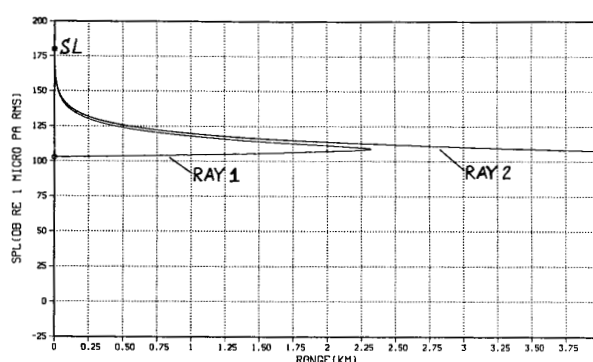


Fig. 5. Sound-pressure level (SPL) plot for test case 1. Source level $SL = 180 \text{ dB re } 1 \mu\text{Pa (rms)}$. Ideal pressure-release surface and ideal rigid bottom.

SPL: RECURSIVE RAY ACOUSTICS

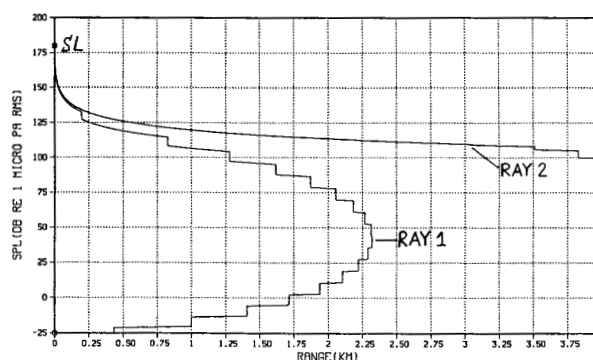


Fig. 6. Sound-pressure level (SPL) plot for test case 2. Source level $SL = 180 \text{ dB re } 1 \mu\text{Pa (rms)}$. Pressure-release surface and viscous fluid bottom.

at $f = 250 \text{ Hz}$; and $\rho_3 = 2070 \text{ kg/m}^3$, $c_3 = 1730 \text{ m/s}$, and $\alpha_3(f) = 0.5 \times 10^{-1} \text{ dB/m}$ ($0.576 \times 10^{-2} \text{ Np/m}$) at $f = 250 \text{ Hz}$. The critical angle of incidence measured with respect to the local normal at the ocean bottom is $\zeta_c = 60.1^\circ$.

Fig. 4 is still applicable as the ray trace for test case 2; however, Fig. 6 illustrates the corresponding SPL plots. For the parameter values given for test case 2, $|R_{21}|$ was equal to unity for all angles of incidence for all practical purposes, resulting in total surface reflections. Since the angle of incidence ζ_{inc} for each bottom reflection that ray 1 ($\beta_0 = 55^\circ$) underwent never exceeded 52° , the corresponding SPL plot shown in Fig. 6 suffered a finite, discontinuous drop in value after each bottom reflection because the magnitude of the ocean bottom reflection coefficient is significantly less than one in value for $\zeta_{\text{inc}} < \zeta_c = 60.1^\circ$ (see Fig. 7). Note that SPL values below -25 dB were set equal to -25 dB for simulation purposes. In contrast, the angle of incidence $\zeta_{\text{inc}} > \zeta_c$ for each bottom reflection that ray 2 ($\beta_0 = 80^\circ$) underwent, except for the last two bottom reflections where $\zeta_{\text{inc}} = 59^\circ$ and 53° , respectively, which are less than $\zeta_c = 60.1^\circ$. As a result, for those bottom

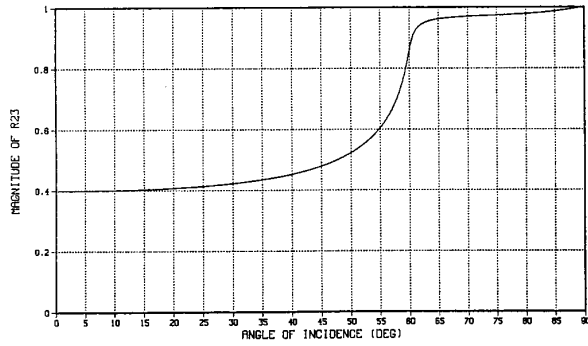


Fig. 7. Magnitude of the ocean bottom reflection coefficient R_{23} versus angle of incidence ζ_{inc} for test case 2. A critical angle of incidence exists at $\zeta_c = 60.1^\circ$.

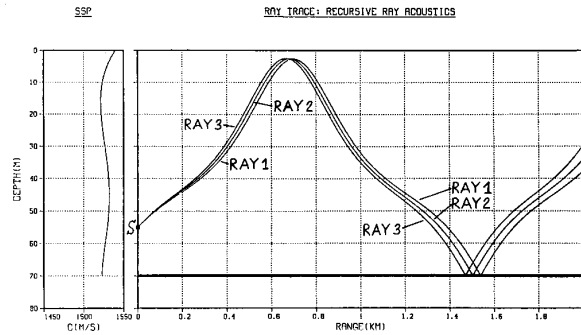


Fig. 8. Ray trace for test case 3. Sound source (S) at a depth of $y_0 = 55$ m. Three rays are transmitted with initial angles of propagation $\beta_0 = 94.2^\circ$ (ray 1), 94.3° (ray 2), and 94.4° (ray 3).

reflections where $\zeta_{inc} > \zeta_c$, the magnitude of the ocean bottom reflection coefficient is approximately equal to one (see Fig. 7), resulting in near total reflection with no visible finite discontinuities in SPL for the range of SPL values plotted. However, if one were to check the actual computer output data, one would find small, finite discontinuities since $|R_{23}| < 1$ for $\zeta_{inc} > \zeta_c$ because of frequency-dependent attenuation.

Test case 3 simulated ray propagation in an ocean waveguide with a *focal point problem* for the calculation of SPL. The ocean surface and bottom were once again modeled as ideal pressure-release and rigid boundaries, with reflection coefficients $R_{21} = -1$ and $R_{23} = 1$, respectively.

The ocean medium was modeled as being nonviscous with the sound-speed profile shown in Fig. 8. The sound source was placed at a depth of $y_0 = 55$ m with a $SL = 180$ dB re $1 \mu\text{Pa}$ (rms). Three rays were transmitted from the source with initial angles of propagation $\beta_0 = 94.2^\circ$, 94.3° , and 94.4° .

An arc length step size of 0.5 m was used. Figs. 8 and 9 illustrate the corresponding ray trace and SPL plots for test case 3. Fig. 9 correctly shows a dramatic increase in SPL for the three rays at the location of the focal points.

V. SUMMARY

Sound-pressure level (SPL) calculations were made along individual ray paths for arbitrary, one-dimensional, depth-

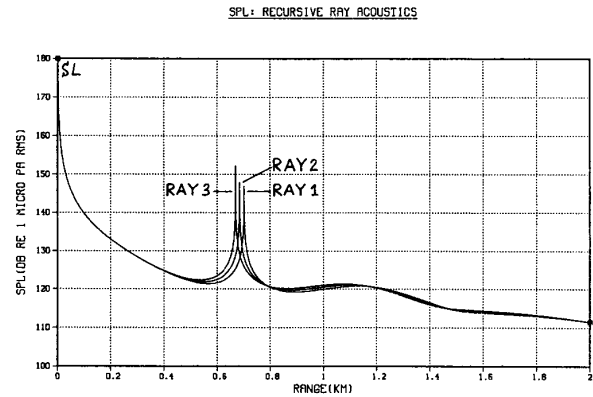


Fig. 9. Sound-pressure level (SPL) plot for test case 3. Source level $SL = 180$ dB re $1 \mu\text{Pa}$ (rms). Ideal pressure-release surface and ideal rigid bottom.

dependent speeds of sound using an enhanced version of the RRA (recursive ray acoustics) algorithm. Computer simulation results from test cases 1 and 2 demonstrated the effects of surface and bottom reflections on SPL values. Computer simulation results from test case 3 demonstrated that valid (i.e., finite) SPL calculations can be made at turning points and focal points without the use of Airy functions. It was also demonstrated that unevenly spaced, noise-corrupted and/or imprecise sound speed versus depth and bathymetric data can be represented by orthogonal function expansions.

APPENDIX

Fig. 10 illustrates a slice through a ray tube where r is the horizontal range. An omnidirectional point source is located at depth y_0 , producing an axisymmetric acoustic field. If we invoke conservation of energy, then

$$I_{avg}(r, y) dS = I_{avg}(r_1, y_1) dS_1 \quad (A1)$$

where $I_{avg}(\cdot)$ is the time-average intensity, and dS_1 and dS are the infinitesimal wavefront surface areas at the beginning and end of the ray tube, respectively, created by rotating the ray tube slice illustrated in Fig. 10, 360° around the Y axis. If both the speed of sound and the equilibrium (ambient) density are only functions of depth y , then

$$I_{avg}(r, y) = \frac{|p(r, y)|^2}{2\rho_0(y)c(y)}. \quad (A2)$$

In order to proceed further, we need expressions for dS_1 and dS .

By referring to Fig. 10, we can write that

$$dS_1 = 2\pi r_1 dl_1 \quad (A3)$$

where $2\pi r_1$ is the circumference of a circle with radius

$$r_1 = R_0 \sin \beta_0, \quad (A4)$$

$\beta_0 = \beta(y_0)$ is the initial angle of propagation at the source depth y_0 , and

$$dl_1 = R_0 d\beta_0 \quad (A5)$$

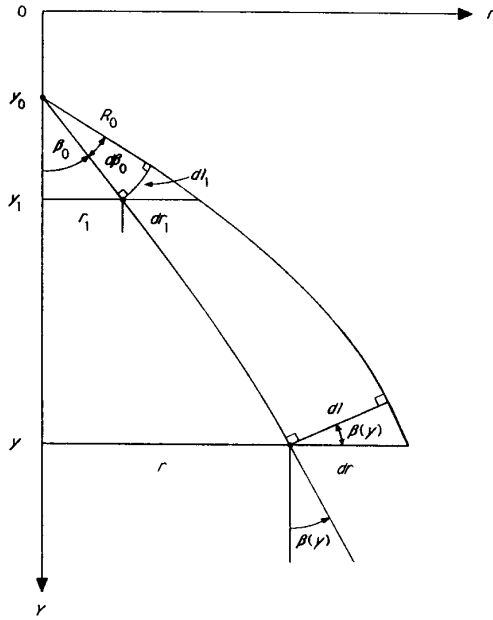


Fig. 10. Illustration of a slice through a ray tube.

is an infinitesimal element of arc length along the wavefront that passes through the point (r_1, y_1) . Therefore, substituting (A4) and (A5) into (A3) yields

$$dS_1 = 2\pi R_0^2 \sin \beta_0 d\beta_0. \quad (\text{A6})$$

Also note that

$$y_1 = y_0 + R_0 \cos \beta_0. \quad (\text{A7})$$

Similarly,

$$dS = 2\pi r dl \quad (\text{A8})$$

where $2\pi r$ is the circumference of a circle with radius r and

$$dl = \cos \beta(y) dr \quad (\text{A9})$$

is an infinitesimal element of arc length along the wavefront that passes through the point (r, y) . Substituting (A9) into (A8) yields

$$dS = 2\pi r \cos \beta(y) dr. \quad (\text{A10})$$

Therefore, upon substituting (A2), (A6), and (A10) into (A1), we obtain the following expression for the magnitude squared of the acoustic pressure along a ray path:

$$|p(r, y)|^2 = |p(r_1, y_1)|^2 \frac{\rho_0(y)c(y)}{\rho_0(y_1)c(y_1)} \frac{R_0^2 \sin \beta_0}{|\cos \beta(y) dr/d\beta_0|} \quad (\text{A11})$$

where the magnitude of $\cos \beta(y) dr/d\beta_0$ is taken in order to ensure that the magnitude squared of the acoustic pressure is positive.

REFERENCES

- [1] L. J. Ziomek and F. Wynn Polnicky, "The RRA algorithm: Recursive ray acoustics for three-dimensional speeds of sound," *IEEE J. Oceanic Eng.*, vol. 18, pp. 25–30, 1993.
- [2] L. Brekhovskikh and Yu. Lysanov, *Fundamentals of Ocean Acoustics*, 1st ed. Berlin: Springer-Verlag, 1982, pp. 38–42.
- [3] C. A. Boyles, *Acoustic Waveguides*. New York: Wiley, 1984, pp. 204–211, 227–230.
- [4] H. R. Krol, "Intensity calculations along a single ray," *J. Acoust. Soc. Amer.*, vol. 53, pp. 864–868, 1973.
- [5] M. B. Porter and H. P. Buckner, "Gaussian beam tracing for computing ocean acoustic fields," *J. Acoust. Soc. Amer.*, vol. 82, pp. 1349–1359, 1987.
- [6] —, "Applications of Gaussian beam tracing to two- and three-dimensional problems in ocean acoustics," in *Proc. 12th World Congr. Sci. Computation*, R. Vichnevetsky et al., Eds., Paris, 1988, pp. 227–230.
- [7] W. Kaplan, *Advanced Mathematics for Engineers*. Reading, MA: Addison-Wesley, 1981, pp. 165–166.

Lawrence J. Ziomek (SM'92) was born in Chicago, IL, on August 8, 1949. He received the B.E. degree in electrical engineering from Villanova University, Villanova, PA, in 1971, the M.S. degree in electrical engineering from the University of Rhode Island, Kingston, RI, in 1974, and the Ph.D. degree in acoustics from the Pennsylvania State University, University Park, PA, in 1981.

From November 1973 to May 1976 he was a member of the Technical Staff at TRW Systems Group, Redondo Beach, CA, and from September 1976 to April 1982 he was a Research Assistant in the Department of Ocean Technology, Applied Research Laboratory, Pennsylvania State University, State College, PA. Since May 1982 he has been with the Naval Postgraduate School, Monterey, CA, where he is currently an Associate Professor in the Department of Electrical and Computer Engineering. His research interests are in underwater acoustics, specifically in theoretical and numerical modeling of pulse propagation and scattering in random media. He is the author of the textbook, *Underwater Acoustics—A Linear Systems Theory Approach* (Orlando, FL: Academic, 1985). He also contributed an invited paper entitled, "Underwater Acoustics" to *The Encyclopedia of Physical Science and Technology*, R. A. Meyers, Editor-in-Chief (Orlando, FL: Academic, 1987).

Dr. Ziomek is a member of the Acoustical Society of America, Eta Kappa Nu, Tau Beta Pi, Sigma Xi, and Phi Kappa Phi.